Polymer 50 (2009) 2933–2943

Contents lists available at ScienceDirect

Polymer

journal homepage: www.elsevier.com/locate/polymer

Synthesis and properties of sulfonated multiblock copolynaphthalimides

Zhaoxia Hu [a], Yan Yin [b], Kazuaki Yaguchi [a], Nobutaka Endo [a], Mitsuru Higa [a], Ken-ichi Okamoto [a,*]

[a] Graduate School of Science & Engineering, Yamaguchi University, Tokiwadai 2-16-1, Ube, Yamaguchi 755-8611, Japan
[b] Tianjin University, Weijin Road 92, Nankai Dis, Tianjin 30072, PR China

ARTICLE INFO

Article history:
Received 13 December 2008
Received in revised form
4 April 2009
Accepted 22 April 2009
Available online 3 May 2009

Keywords:
Multiblock sulfonated co-polyimide
Anisotropic proton conductivity
Microphase-separated morphology

ABSTRACT

Sulfonated multiblock copolynaphthalimides (co-SPIs) with block length of 5–20 were prepared by a two-pot polymerization method from 1,4,5,8-naphthalenetetracarboxylic dianhydride, sulfonated diamines of 2,2′-bis(4-sulfophenoxy)benzidine (BSPOB) and 4,4′-bis(4-aminophenoxy)biphenyl-3,3′-disulfonic acid (BAPBDS) and nonsulfonated diamines. The scanning transmission electron microscopy showed that the BSPOB-based multiblock co-SPI membranes had well-defined microphase-separated structure where the hydrophilic and hydrophobic layer-like domains were oriented in the plane direction of membrane. On the other hand, the BAPBDS-based multiblock co-SPIs and all the random co-SPIs showed the homogeneous morphology. The water uptake, anisotropic membrane swelling, anisotropic proton conductivity and polymer electrolyte fuel cell (PEFC) performance were investigated for the multiblock and random co-SPIs. The results demonstrated strong effects of the membrane morphology on these properties. The BSPOB-based multiblock co-SPI membranes exhibited the larger *through-plane* swelling and the lower *through-plane* conductivity than the random ones, and as a result exhibited the lower PEFC performances. This study gives good understanding of the morphology–property relationship in novel block architectures' design.

1. Introduction

The research on polymer electrolyte fuel cells (PEFCs) has been drawing great attention since the world-wide energy crisis in the last century. Both the environmental friendship and the high efficiency have been the outstanding merits of PEFCs [1,2]. Polymer electrolyte membrane (PEM) is a key component playing a critical role on PEFC performance, and requires high proton conductivity, long physical and chemical stability and low cost. Recently, sulfonated aromatic polymers have been recognized as alternative PEM materials to the state-of-the-art perfluorosulfonic acid polymers such as Nafion [3–7].

Proton conductivity and membrane swelling behavior of PEMs are two important factors in achieving high electrochemical performance for PEFCs and are generally controlled not only by its chemical structure but also by the morphology. It is widely accepted that the hydrophilic–hydrophobic microphase-separated structure is favorable for achieving better proton conductivity than the homogeneous structure. For PEFC applications, the *through-plane* proton conductivity (namely the conductivity in thickness direction of membrane) is much more important than the *in-plane* conductivity (namely the conductivity in plane direction). However, so far, most reports have dealt with only the *in-plane* conductivity because of the difficulty in measuring the *through-plane* conductivity. Only a few reports have dealt with the *through-plane* conductivity [7–12]. As for the membrane swelling, the *in-plane* swelling is required to be low to achieve the good adhesive and mechanical stability of membrane electrode assembly (MEA). Therefore, it is important to investigate the relationship among the chemical structure, morphology and properties for PEMs.

Good proton conduction performance of Nafion membranes is closely related to the special morphology of ion-cluster channel structures [2,13]. They exhibit the isotropic proton conductivity and isotropic membrane swelling [10].

Diblock, triblock and graft copolymers composed of sulfonated polystyrene blocks and fluorinated or nonfluorinated polyalkylene blocks, of which typical chemical structures are shown in Fig. 1, have been intensively studied on the membrane morphology by means of transmission electron microscopy (TEM), small-angle X-ray scattering and tapping-mode atomic force microscopy (TM-AFM) in connection with the proton conductivity. The cross-sectional TEM images revealed that the dry membranes had hydrophilic–hydrophobic microphase-separated structures with spherical, lamellar or wormlike morphology [11,12,14–18]. These block copolymers exhibited much higher *in-plane* proton conductivity than the randomly sulfonated polystyrene with the similar ion exchange capacities (IECs) [15,17,18]. Elabd et al. measured the *through-plane*

* Corresponding author. Tel.: +81 836 85 9660; fax: +81 836 85 9601.
E-mail address: okamotok@yamaguchi-u.ac.jp (K.-i. Okamoto).

0032-3861/$ – see front matter © 2009 Elsevier Ltd. All rights reserved.
doi:10.1016/j.polymer.2009.04.040

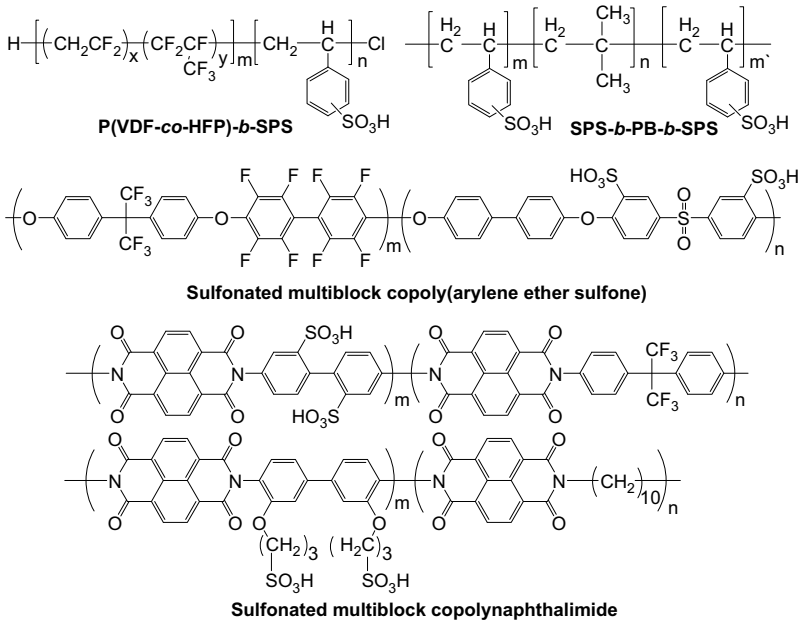

Fig. 1. Chemical structures of typical block copolymers.

conductivity in the fully hydrated state for sulfonated poly(styrene-*b*-isobutylene-*b*-styrene) triblock copolymers as a function of IEC ranging from 0.5 to 2.0 meq g^{-1} [11]. They found a discontinuous jump of the *through-plane* conductivity around an IEC of 1.0 meq g^{-1} due to a morphological transition. At lower IEC range of 0.5–1.0 meq g^{-1}, the membranes showed an anisotropic lamellar morphology oriented in the plane direction of membrane and as a result had the lower *through-plane* conductivity, whereas at higher IEC range of 1.1–2.0 meq g^{-1} they showed an isotropic continuous morphology and had the much higher *through-plane* conductivity. Their *through-plane* conductivity at the higher IEC range was about one order of magnitude higher than that of sulfonated polystyrenes. Holdcroft et al. measured both the *through-plane* and *in-plane* proton conductivity for graft and diblock copolymers composed of partially sulfonated polystyrene block and poly(vinylidene difluoride-*co*-chlorotrifluoroethylene) block [12]. The graft copolymers exhibited the morphology characterized by an interconnected network of small ionic clusters, resulting in the lower water uptake and the isotropic proton conductivity with the similar *through-plane* and *in-plane* conductivity. On the other hand, the diblock copolymers exhibited well-segregated lamellar morphology, resulting in the lamellar-like nature of membrane. They exhibited the higher water uptake especially for IEC $>$ 1.0 meq g^{-1} and the anisotropic proton conductivity with 2.4 times smaller *through-plane* conductivity than *in-plane* conductivity. These research works point out that it is important to consider the effect of morphology on *through-plane* conductivity in the design of novel membranes based on block architectures.

Multiblock aromatic copolymers composed of sulfonated hydrophilic and nonsulfonated hydrophobic blocks have been studied to enhance the proton conductivity [19–27]. Compared with the polymers mentioned above, sulfonated aromatic polymers have relatively rigid polymer backbone. Therefore, it is not easy to observe clearly phase-separated structure for the dry membranes by means of TEM. In most studies, the surface morphology for the hydrated membranes has been investigated by means of TM-AFM. McGrath et al. have reported on multiblock sulfonated–fluorinated poly(arylene ether)s (MBs) [21]. MB-150 having hydrophilic/hydrophobic block lengths of about 8/8 and IEC of 1.5 meq g^{-1} showed a perfect phase-separated surface morphology and very high *in-plane* conductivity under the low relative humidity (RH), for example, 25 mS cm^{-1} at 30 °C and 50% RH. This was much higher than the sulfonated poly(ether sulfone) random copolymers. Recently, Ueda et al. developed multiblock copoly(ether sulfone)s with high molecular weights using a chain extender, which showed well phase-separated surface morphology and higher *in-plane* conductivity than the random copolymers [27]. Their multiblock copolymers showed the mild anisotropic membrane swelling with larger swelling in the thickness direction than in the plane direction, whereas the random copolymers showed the isotropic membrane swelling.

Sulfonated polynaphthalimides (SPIs) derived from 1,4,5,8-naphthalenetetracarboxylic dianhydride (NTDA) and sulfonated and nonsulfonated diamines have more rigid backbone than the sulfonated poly(arylene ether)s mentioned above. Pineri et al. studied on sequenced co-SPI membranes derived from NTDA, 4,4′-diaminobiphenyl-2,2′-disulfonic acid (BDSA) and oxydianiline (ODA) [8]. The *through-plane* conductivity depended on the hydrophilic sequence length and a maximum was observed for a short sequence length of 3. The SPI with a long sequence of 9 showed a smaller *through-plane* conductivity. The co-SPI membranes showed the anisotropic membrane swelling with 3.5–11 times larger swelling in the thickness direction than in the plane direction. On the other hand, other research groups investigated the effect of block length on the *in-plane* conductivity for block co-SPIs [28–30]. Kawakami et al. prepared block co-SPIs derived from NTDA, BDSA and 4,4′-diaminophenyl hexafluoropropane (BAHF) with a high IEC of 2.4 meq g^{-1} [28,29]. Their block co-SPI with long hydrophilic/hydrophobic block lengths of 140/60 showed largely improved *in-plane* conductivity, for example 20 mS cm^{-1} at 80 °C and 50% RH, whereas the one with block lengths of 70/30 showed the low *in-plane* conductivity similar to that of the random co-SPI. Watanabe et al. reported that a block co-SPI derived from NTDA, 3,3′-bis(sulfopropoxy)benzidine (BSPB) and 1,10-decamethylenediamine having long block lengths of 150/150 and an IEC of 1.8 meq g^{-1} showed very high *in-plane* conductivity; for example 20 mS cm^{-1} at 80 °C and 50% RH, which was ten times higher than that of the random co-SPI [30]. These results are different from the former results. Furthermore, the latter groups did not deal with the *through-plane* proton conductivity and the membrane swelling behavior.

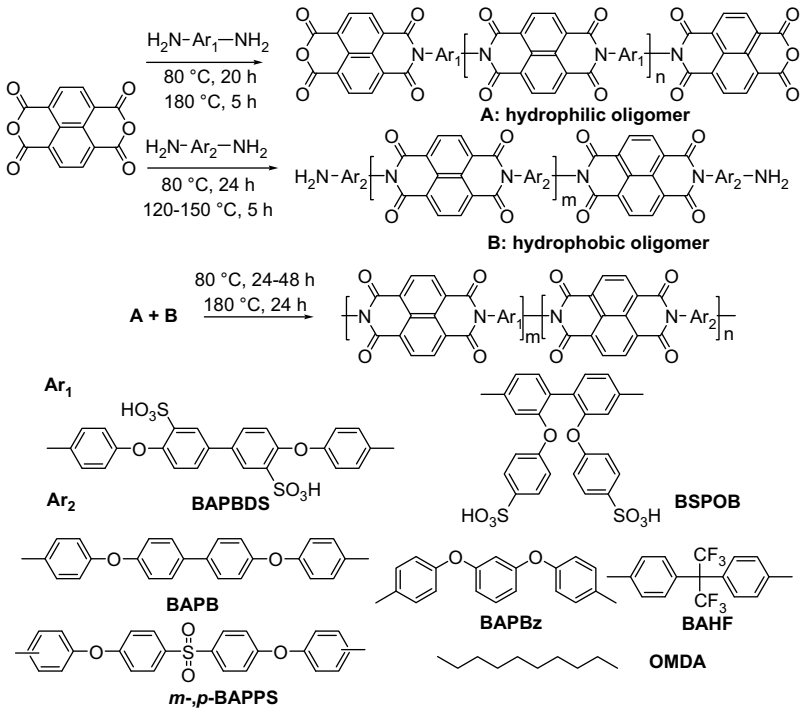

Scheme 1. Synthesis of NTDA-based multiblock co-SPIs.

Judging from the results mentioned above, it is very important for evaluation as PEMs to investigate the cross-sectional morphology of membrane as well as the proton conductivity and membrane swelling in both the thickness and plane directions for multiblock aromatic copolymers. This is essentially required for multiblock co-SPIs, because the random and sequenced co-SPIs have been reported to show the strong anisotropic membrane swelling behavior [7,8,31–36]. In this study, the physical properties including proton conductivity, membrane swelling and their anisotropy, the cross-sectional morphology and PEFC performance are investigated for multiblock and random co-SPI membranes.

2. Experimental section

2.1. Materials

4,4′-Bis(4-aminophenoxy)biphenyl-3,3′-disulfonic acid (BAPBDS) and 2,2′-bis(4-sulfophenoxy)benzidine (BSPOB) were prepared according to the methods previously reported [31–33]. NTDA was purified by vacuum sublimation. 4,4′-Bis(4-aminophenoxy)biphenyl (BAPB), 1,3-bis(4-aminophenoxy)benzene (BAPBz), BAHF, 4,4′-bis(4-diaminophenoxy)diphenylsulfone (*p*BAPPS), 4,4′-bis(3-diaminophenoxy)diphenylsulfone (*m*BAPPS) and 1,8-octamethylenediamine (OMDA) were purchased from Tokyo Kasei Co. and recrystallized from ethanol before use. Triethylamine (TEA) was purified by distillation under reduced pressure and dehydrated with 4 Å molecular sieves. Benzoic acid, isoquinoline, sulfuric acid (95%), fuming sulfuric acid (60%), methanol, *m*-cresol and other reagents were used as received. Ultra-pure water was obtained from a Millipore Milli-Q purification system.

2.2. Synthesis of multiblock co-SPIs

Multiblock co-SPIs were synthesized by a two-pot method as described in Scheme 1. As an example, the synthesis of NTDA–BSPOB/BAHF (20/20), where the figures in the parentheses refer to the hydrophilic/hydrophobic block lengths, is described below.

An anhydride-end-capped hydrophilic oligomer was synthesized as follows. To a completely dried 200 mL four-necked flask equipped with a mechanical stirrer, a condenser and nitrogen inlet/outlet were charged 3.319 g (6.28 mmol) of BSPOB, 25 mL of *m*-cresol and 2.4 mL of TEA. After BSPOB completely dissolved, 1.771 g (6.60 mmol) of NTDA and 1.128 g of benzoic acid were added to the flask. With mechanically stirring, the reaction solution was heated at 80 °C for 20 h and then at 180 °C for 5 h, and cooled to room temperature.

An amine-end-capped hydrophobic oligomer was synthesized as follows. To a completely dried 100 mL three-necked flask equipped with a condenser and nitrogen inlet/outlet were charged 2.099 g (6.28 mmol) of BAHF and 36 mL of *m*-cresol. After BAHF completely dissolved, 1.598 g (5.96 mmol) of NTDA and 1.108 g of benzoic acid were added to the flask. With magnetically stirring, the reaction solution was heated at 80 °C for 24 h and then at 120–150 °C for 5 h, and cooled to room temperature.

The hydrophobic block oligomer solution was very carefully added to the 200 mL four-necked flask to mix with the hydrophilic oligomer solution, and additional amount of *m*-cresol was added to the flask to maintain solid content of the reaction system at 10–15 wt%. With stirring, the reaction mixture was kept at 80 °C for 24–48 h and at 180 °C for 12 h, and 2.364 g of isoquinoline was added and the reaction was continued for another 12 h, and then cooled to 80 °C. After 20 mL of *m*-cresol was added to dilute the viscous solution, the mixture was poured into a large amount of acetone. The precipitated fiber-like polymer was filtrated, washed with acetone several times and dried *in vacuo* at 80 °C for 10 h.

2.3. Membrane formation and characterization

SPI in TEA salt form was dissolved in *m*-cresol with a concentration of 5–6 wt%. After filtration, the filtrate was cast onto glass plates and the temperature was raised up to 120 °C and kept for 10 h. The as-cast membranes were soaked in methanol at 40 °C for

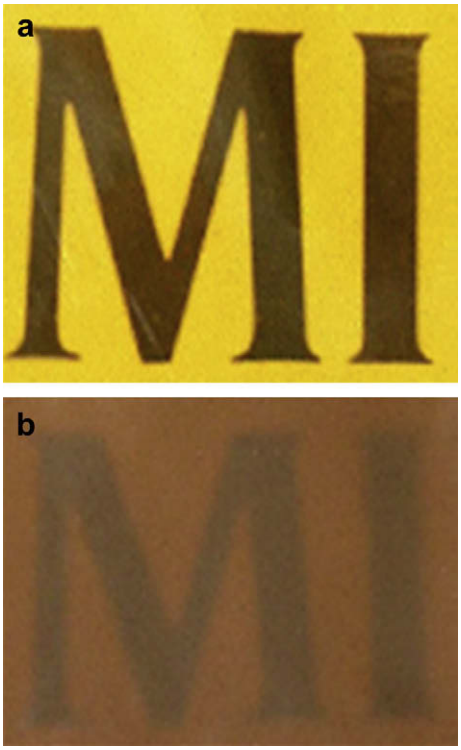

Fig. 2. Photographs of transparent and opaque multiblock co-SPI membranes. (a) NTDA–BAPBDS/BAHF (20/10) (B5), (b) NTDA–BAPBDS/BAPB (10/5) (B1).

48 h and then proton-exchanged with 1.0 M hydrochloric acid at 50 °C for 72 h. The proton-exchanged membranes were thoroughly washed with water and then cured using stainless steel frames *in vacuo* at 150 °C for 1 h and then at 180 °C for 1 h. The SPI membranes obtained were 40–70 μm in thickness.

FT-IR spectra were recorded on a Horiba FT-200 Spectrometer by ATR (attenuated total reflection). Thermogravimetry (TG) analysis was performed on Rigaku TG-8120 in helium (flow rate: 100 $cm^3\,min^{-1}$) at a heating rate of 10 °C min^{-1}. The reduced viscosity η_r was measured with an Ostwald viscometer with 0.5 g dL^{-1} *m*-cresol solution at 35 °C. Mechanical tensile tests were performed on a universal testing machine (Orientic, TENSILON TRC-1150A) at 25 °C and around 60% RH. Scanning electron microscopy (SEM) was performed using a JEOL JSM-6335F instrument. Scanning transmission electron microscopy (STEM) was performed using an HITACHI STEM (HD-2000) instrument. Membranes were stained with cesium ions. Samples (cross-sectional slices 50–100 nm thick) were prepared using a cryomicrotome.

Ion exchange capacities (IECs) were determined by the titration method, which were compared with the theoretical values calculated from the feed molar ratio of sulfonated diamine to non-sulfonated diamine. A sample membrane in proton form was soaked in a 15 wt% NaCl solution for 48–72 h at 30 °C to exchange the H^+ ion with Na^+ ion. Then the H^+ ion released into the solution was titrated with a 0.02 N NaOH solution using phenolphthalein as an indicator.

Water uptake (WU), and dimensional change in membrane thickness (Δt_c) and plane direction (Δl_c) were measured according to the method described elsewhere [31]. Water uptake was measured by soaking a sample sheet into water at 30 °C for 5 h. Then the membrane was taken out, wiped with tissue paper very quickly, and weighed on a microbalance. Water uptake was calculated from Eq. (1):

$$\mathrm{WU} = (W_s - W_d)/W_d \times 100\% \quad (1)$$

where W_d and W_s are the weights of dry and corresponding water-swollen membranes, respectively.

Dimensional change of SPI membrane was measured by soaking more than two sample sheets in water at 30 °C for 5 h. The *through-plane* and *in-plane* dimensional changes and the anisotropic membrane swelling ratio ($\Delta_{t/l}$) were calculated from Eq. (2):

$$\Delta t_c = (t - t_s)/t_s$$

$$\Delta l_c = (l - l_s)/l_s$$

$$\Delta_{t/l} = \Delta t_c/\Delta l_c \quad (2)$$

where t_s and l_s are the thickness and length of the membrane equilibrated at 70% RH, respectively; t and l refer to those of the membrane immersed in water.

In-plane and *through-plane* proton conductivity ($\sigma_{\parallel}$ and $\sigma_{\perp}$, respectively) of SPI membrane was determined using an electrochemical impedance spectroscopy technique over the frequency from 10 Hz to 100 kHz (Hioki 3532-80). For $\sigma_{\parallel}$, a single cell with two

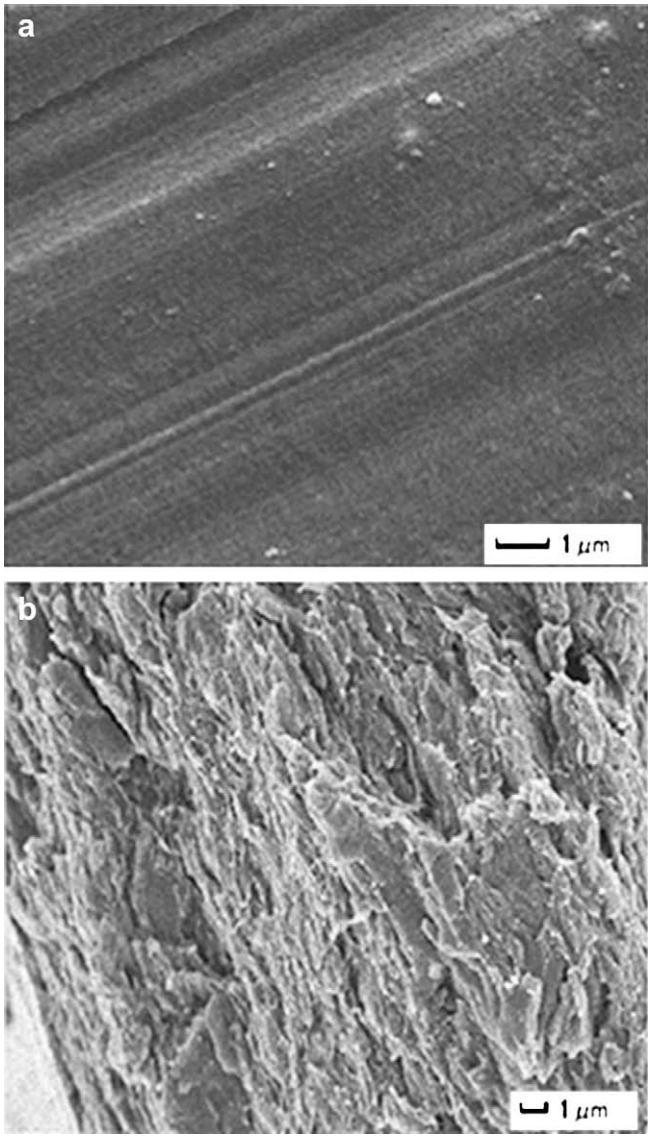

Fig. 3. SEM images of multiblock co-SPI membranes. (a) NTDA–BAPBDS/BAHF (20/10) (B5), (b) NTDA–BAPBDS/BAPB (10/5) (B1).

Table 1
Properties of multiblock and random co-SPIs.

Code	NTDA-based co-SPIs	IEC[a] (meq g^{-1})	η_r[b] (dL g^{-1})	WU[c] (g 100 g^{-1})	λ	Dimensional change[c]		$\sigma_{\parallel}$[d] (mS cm^{-1})		
						Δt_c	Δl_c	50%	70% RH	In water
B1[e]	BAPBDS/BAPB (10/5)	1.89 (1.66)	1.6	62	18	0.24	0.112	6.3	22	142
B2[e]	BAPBDS/*p*BAPPS (10/5)	1.89 (1.61)	1.4	55	17	0.15	0.084	6.2	28	125
B3[e]	BAPBDS/BAPBz (10/6.7)	1.80	2.2	62	19	0.18	0.077	4.9	20	121
B4[e]	BAPBDS/OMDA (10/10)	1.76	2.1	55	17	0.15	0.100	5.3	18	104
B5	BAPBDS/BAHF (20/10)	1.92 (1.79)	2.7	79	23	0.34	0.102	11	36	179
B6	BAPBDS/BAHF (20/13.3)	1.76	1.6	65	21	0.24	0.066	7.3	22	139
B7	BAPBDS/BAHF (20/20)	1.51 (1.44)	2.2	56	21	0.25	0.069	6.9	25	123
B8	BSPOB/BAHF (20/20)	1.51 (1.42)	2.2	76	28	0.48	0.019	10	39	156
B9	BSPOB/*m*BAPPS (10/10)	1.40	4.1	60	24	0.31	0.013	8.0	31	120
B10	BSPOB/*m*BAPPS (20/20)	1.40	2.5	55	22	0.36	0.015	6.6	31	135
R1	BAPBDS/BAPB (2/1)	1.89 (1.86)	4.4	57	17	0.14	0.049	5.0	29	127
R2	BAPBDS/BAPBz (1/1)	1.56	4.0	44	16	0.09	0.034	3.8	16	78
R3	BSPOB/BAPBz (2/1)	1.96 (1.84)	9.9	76	22	0.40	0.036	8.6	33	178
R4	BSPOB/BAHF (1/1)	1.51 (1.42)	4.9	57	21	0.27	0.029	5.0	24	99
R5	BSPOB/*m*BAPPS (1/1)	1.40 (1.36)	3.0	45	18	0.16	0.027	3.4	16	80
	Nafion 112	0.91		39	24	0.13	0.12	26	52	139

[a] Calculated data, data in the parentheses refer to titration method.
[b] At 35 °C with 0.5 wt% solution in *m*-cresol.
[c] At 30 °C.
[d] At 60 °C.
[e] Opaque membranes.

platinum plate electrodes was mounted on a Teflon plate at 0.5 cm distance. The cell was placed under either in a thermo-controlled humidic chamber or in liquid water [34]. For $\sigma_{\perp}$, a membrane sample was set between two platinum plate electrodes of 1 cm^2 area, and mounted on two Teflon blocks. The cell was placed in liquid water. Proton conductivity ($\sigma_{\parallel}$ and $\sigma_{\perp}$) and the anisotropic proton conductivity ratio ($\sigma_{\perp/\parallel}$) were calculated from Eq. (3):

$$\sigma_{\parallel} = d/(t_s w_s R)$$

$$\sigma_{\perp} = t_s/(AR)$$

$$\sigma_{\perp/\parallel} = \sigma_{\perp}/\sigma_{\parallel} \quad (3)$$

where d is the distance between the two electrodes, t_s and w_s are the thickness and width of the membrane at a standard condition of 70% RH, respectively, A is the electrode area, and R is the resistance value measured. The thickness of a water-swollen membrane was used in the calculation of both $\sigma_{\parallel}$ and $\sigma_{\perp}$ in the fully hydrated state. The *through-plane* conductivity measurement was performed only on the cell placed in water, because the contact resistance between electrodes and membrane could be neglected only in the fully hydrated state. The similar $\sigma_{\perp}$ values were obtained for the samples of single layer and double layers of membrane.

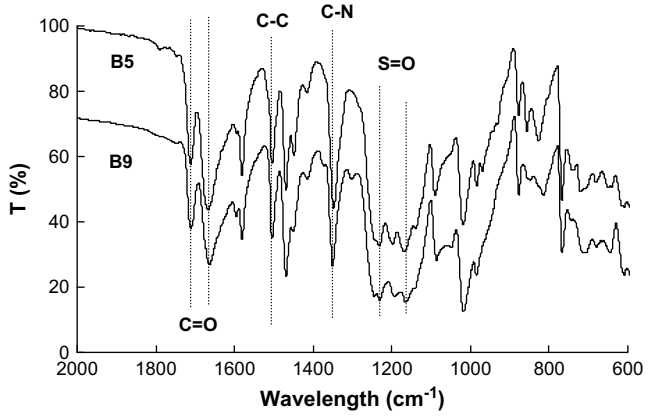

Fig. 4. FT-IR spectra of multiblock co-SPIs.

2.4. Fuel cell performance measurement

An MEA was fabricated from an SPI membrane (4.5 cm × 4.5 cm) sample by hot-pressing an electrode/membrane/electrode sandwich at 150 °C for 5 min under 60 kg cm^{-2}. The effective electrode area was 5 cm^2. Prior to the hot-pressing, both surfaces of the membrane and catalyst electrodes (Johnson and Matthey) were impregnated with 1.25 or 5 wt% Nafion solution as binder. The MEA was set in a single-cell test fixture (NF Inc., active area: 5 cm^2) and mounted in an in-house fuel cell station (NF Inc., model As-510), which was supplied with temperature-controlled humidified gases (H_2 and air). The PEFC performance was evaluated at a cell temperature of 90 °C, a gas pressure of 0.3 MPa and gas humidifier temperatures of 85, 72 and 59 °C, corresponding to 84, 50 and 30% RH, respectively. The gas flow was controlled to keep constant utilization of H_2 at 70% and of air at 15% and 30% at a humidification temperature of 85 °C and 72 °C, respectively, although the lowest gas flow rate was limited at 30 N cm^3 min^{-1}. At a humidification temperature of 59 °C, the utilization of H_2 and air was kept at 80% and 50%, respectively.

3. Results and discussion

3.1. Synthesis and characterization

A multiblock co-SPI was synthesized by a two-pot method as described in Scheme 1. In the first stage, an anhydride-end-capped hydrophilic oligomer and an amine-end-capped hydrophobic oligomer were synthesized separately. Secondly, the oligomer solutions were mixed very carefully and kept at 80 °C for 24–48 h and then at 180 °C for 24 h to react adequately and to obtain high molecular weight polymers. The block length (l) of the hydrophilic and hydrophobic segments was set for 5, 10 or 20 by controlling the feed ratio of NTDA to diamines, which was estimated according to the following Eq. (4):

Table 2
Anisotropy of membrane swelling and proton conductivity for multiblock and random co-SPI membranes.

Code	IEC[a] (meq g^{-1})	Thickness (μm)	WU[b] (g 100 g^{-1})	Size change[b]		$\Delta_{t/l}$	σ[c] (mS cm^{-1})		$\sigma_{\perp/\parallel}$
				Δt_c	Δl_c		$\sigma_\perp$	$\sigma_\parallel$	
B1[e]	1.89	71	62	0.24	0.112	2.2	97	142	0.68
B5	1.92	64	79	0.34	0.102	3.4	97	179	0.54
B7	1.51	65	56	0.25	0.069	3.6	70	123	0.57
B8	1.51	58	76	0.48	0.019	25	33	156	0.21
B9	1.40	66	60	0.31	0.013	24	52	120	0.44
B10	1.40	60	55	0.36	0.015	24	15	135	0.11
R1	1.89	60	57	0.14	0.049	2.9	93	127	0.73
R2	1.56	45	44	0.09	0.034	2.6	60	78	0.77
R3	1.96	42	76	0.40	0.036	11	119	178	0.67
R4	1.51	33	57	0.27	0.029	9.3	60	99	0.61
R5	1.40	54	45	0.16	0.027	6.0	51	80	0.64
Nafion112	0.91	55	39	0.13	0.12	1.1	136	139	0.98

[a] Calculated data.
[b] At 30 °C.
[c] At 60 °C in water.
[e] Opaque membranes.

$$l = (r+1)/2(r-1) \quad (4)$$

where r (>1) refers to the molar ratio of NTDA to sulfonated diamine for hydrophilic oligomer, or the molar ratio of non-sulfonated diamine to NTDA for hydrophobic oligomer.

It should be pointed out that different behaviors were observed for the synthesis of hydrophobic oligomers. The hydrophobic oligomer derived from BAHF or *m*BAPPS was completely soluble in *m*-cresol, resulting in a clear solution of block copolymer and transparent cast membranes. On the other hand, the hydrophobic oligomer derived from other diamine such as BAPB, BAPBz, *p*BAPPS and OMDA did not completely dissolve in *m*-cresol irrespective of the block length of 5–10, resulting in the opaque oligomer solution. Using the opaque oligomer solution, the resulting block copolymer solution was also opaque. Opaque membranes were obtained by casting the opaque solution. Fig. 2 shows the difference in appearance of these two types of membranes. In the SEM observation, as shown in Fig. 3, the transparent membrane of NTDA–BAPBDS/BAHF (20/10) (B5) (code designated in Table 1) showed a homogeneous structure, whereas the opaque membrane of NTDA–BAPBDS/BAPB (10/5) (B1) showed a fibrous inhomogeneous structure. Therefore, we discussed the properties of only the transparent multiblock co-SPI membranes (B5–B10) in details in the following sections.

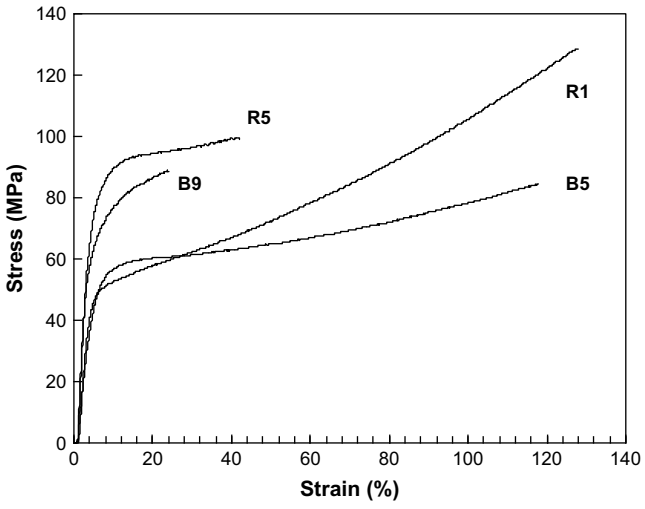

Fig. 5. Stress–strain curves of multiblock and random co-SPI membranes.

Fig. 4 shows the FT-IR spectra of multiblock co-SPI membranes. Typical bands were found at 1709, 1662 and 1349 cm^{-1}, referring to the symmetric, asymmetric vibration of C═O groups and vibration of C–N groups of the six-membered imide rings, respectively. The strong and broad bands for asymmetric and symmetric vibration of O═S═O groups in the sulfonic acid groups appeared at 1210 and 1175 cm^{-1}, respectively. The complete imidization was supported by the absence of absorbance peaks around 1780 and 1820 cm^{-1} assigned to carbonyl groups in anhydride rings, indicating the successful preparation of the multiblock co-SPIs by the two-pot polymerization method in this study.

Table 1 lists the physical properties of the multiblock co-SPIs (B1–B10), together with random co-SPIs (R1–R5) cited for comparison. The IEC values determined by titration method were slightly lower than the theoretical ones. It is noted that the same IEC value was obtained for NTDA–BSPOB/BAHF (1/1) (R4) and NTDA–BSPOB/BAHF (20/20) (B8), a representative pair of random and multiblock co-SPIs, indicating the quantitative reaction of the reagents in block polymerization. It is difficult to measure the molecular weights of the multiblock co-SPIs by the widely used gel permeation chromatography (GPC) method because they were soluble only in *m*-cresol in their TEA salt form. Instead, the reduced viscosities were measured to evaluate the molecular weights of the co-SPIs. The multiblock co-SPIs showed the high reduced viscosities more than 2.2 dL g^{-1}, which were much larger than those of the hydrophilic and hydrophobic oligomers, 0.5–0.6 dL g^{-1} and 0.2–0.3 dL g^{-1}, respectively. These results indicated that the multiblock co-SPIs were successfully prepared. According to the TG analysis, the multiblock and random co-SPI membranes exhibited excellent thermal stability, with the desulfonation temperatures of 300–310 °C.

Comparison of water uptake (or water vapor sorption) is often performed in terms of the number of water molecules sorbed per sulfonic acid group, λ. In this study, the theoretical IEC values were used to calculate λ. Although the water vapor sorption isotherms were not provided here, the λ values were larger for the multiblock co-SPIs than for the random ones. For example, the λ values of B8 were 2.96, 4.71 and 6.94 at 30, 50 and 70% RH, respectively, whereas those of R4 were 2.75, 4.25 and 5.91 respectively. The difference in λ increased from 8% to 18% with increasing RH from 30% RH to 70% RH. The λ values in water were about 30% larger for the multiblock co-SPIs from BSPOB than for the corresponding random co-SPIs (B8 vs. R4; B9 and B10 vs. R5), as listed in Table 1. In the case of BAPBDS-based SPIs, the transparent membranes of the multiblock co-SPIs (B5–B7) showed about 30% larger λ values than

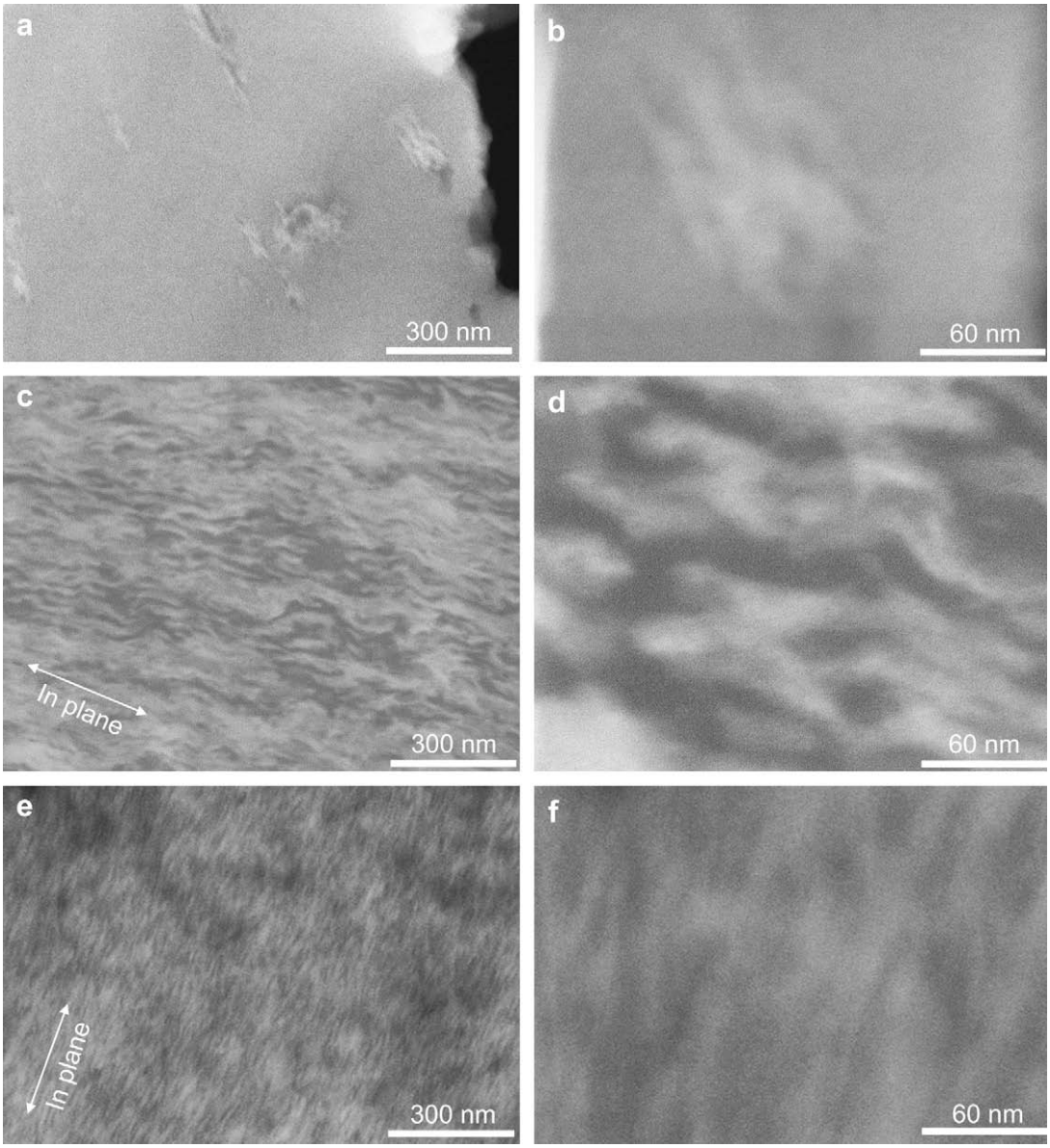

Fig. 6. STEM images of multiblock and random co-SPI membranes stained with Cs^+ ions. (a) and (b) NTDA–BSPOB/BAHF (1/1) (R4); (c) and (d) NTDA–BSPOB/BAHF (20/20) (B8); (e) and (f) NTDA–BSPOB/*m*BAPPS (10/10) (B9).

the random co-SPIs (R1 and R2), but so large differences were not observed for the opaque membranes (B1–B4). Kawakami et al. reported 20–40% larger λ values for the BDSA-based block co-SPIs than for the random co-SPI [28,29].

The *through-plane* and *in-plane* dimensional change (Δt_c and Δl_c, respectively) and the anisotropic membrane swelling ratio ($\Delta_{t/l}$) are summarized in Table 2. All the co-SPI membranes in this study exhibited the anisotropic membrane swelling with larger *through-plane* dimensional changes. The anisotropic membrane swelling is considered due to the polymer chain alignment in plane direction of membrane. The rigid imide backbone from NTDA and benzidine with sulfonated pendants seems to cause the better alignment of polymer chain in plane direction. This is a reason that the BSPOB-based co-SPIs exhibited much larger anisotropic membrane swelling ratio than the BAPBDS-based co-SPIs having two flexible ether bonds in a repeat unit [33]. The evaluation of polymer chain alignment by means of Raman spectroscopy is in progress and will be reported elsewhere.

For the BSPOB-based SPIs, the multiblock co-SPIs showed 30% larger water uptake than the random ones, as mentioned above. This increase in water uptake was followed by an about 2-fold increase in the Δt_c and a slight decrease in Δl_c. As a result, the BSPOB-based multiblock co-SPI membranes showed much larger $\Delta_{t/l}$ values (24–25) than the random ones (6–11). On the other hand, in the case of the BAPBDS-based SPIs, the 30% larger water uptake for the multiblock co-SPIs was followed by increases in both Δt_c and Δl_c. As a result, the BAPBDS-based multiblock co-SPI membranes showed slightly larger $\Delta_{t/l}$ values (around 3.5) than the random ones (2.5–3). This membrane swelling behavior is discussed below based on the membrane morphology.

Fig. 5 shows the stress–strain curves of two typical multiblock co-SPI membranes together with two random ones. The two multiblock co-SPI membranes exhibited high mechanical strength comparable to that of the corresponding random ones (B5 to R1; B9 to R5), for example, large Young's modulus of 1.3 GPa, maximum stress at break of 85 MPa and elongation at break of 120% for B5.

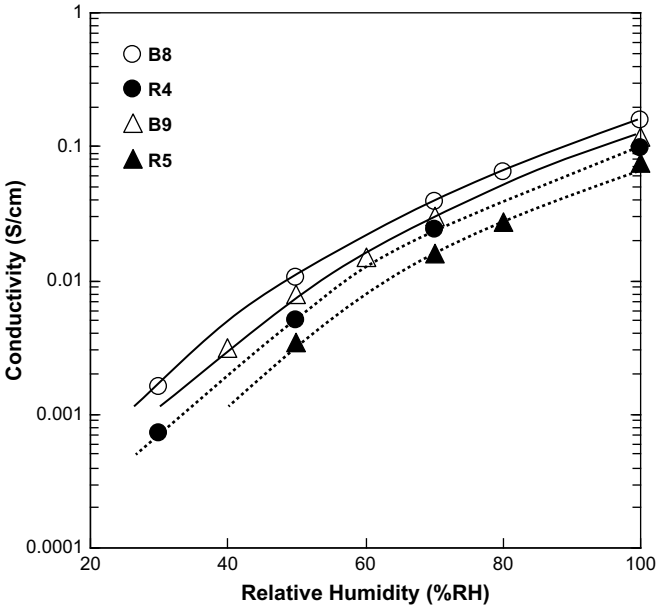

Fig. 7. Relative humidity dependence of *in-plane* proton conductivity for BSPOB-based multiblock and random co-SPI membranes.

3.2. Morphology

STEM observation was performed on the SPI membranes stained with Cs^+ ions. Fig. 6 shows the STEM dark field images for the BSPOB-based multiblock co-SPI membranes, B8 and B9, and the random co-SPI membrane, R4. Simultaneously, spot energy dispersive X-ray (EDX) analysis was performed. The STEM images of R4 in Fig. 6(a) and (b) did not show any contrast, indicating its homogeneous morphology. On the other hand, the STEM images in Fig. 6(c) and (d) for NTDA–BSPOB/BAHF (20/20), B8, exhibited a well-defined microphase-separated structure composed of bright and dark domains. Furthermore, the domains were oriented in the plane direction of membrane to form a layer-like structure. According to the EDX analysis, the element contents of S and Cs were 1.4 and 1.9%, respectively, for the bright parts and 0.2 and 0.3% for the dark parts. The former was much higher than the latter. Therefore, the bright parts referred to the hydrophilic domains and the dark parts referred to the hydrophobic domains. The hydrophilic domains were 10–20 nm in width and interconnected to form ionic channels. The hydrophobic domains were the similar size in width and interconnected to form hydrophobic spaces. These hydrophilic and hydrophobic domains oriented in the plane direction and formed a layer-like structure. This is the first example that the well-defined microphase-separated structure, where the hydrophilic and hydrophobic layer-like domains were oriented in the plane direction, was observed for the cross-section of aromatic PEM. This layer-like structure predicts increases in both the interaction between the interconnected hydrophilic domains and the interaction between the interconnected hydrophobic domains and a decrease in the interaction between hydrophilic and hydrophobic layer-like domains. As a result, it leads to an increase in the *in-plane* proton conductivity and a decrease in the *through-plane* conductivity, whereas it leads to an increase in the *through-plane* membrane swelling and a decrease in the *in-plane* swelling. These predictions are in agreement with the experimental results about the anisotropic membrane swelling and the anisotropic proton conductivity for B8 and R4 as have been mentioned above.

The STEM images in Fig. 6(e) and (f) for NTDA–BSPOB/*m*BAPPS (10/10), B9, exhibited an indistinct microphase-separated structure where the hydrophilic and hydrophobic domains were less defined and no clear difference in the element content was observed by EDX analysis. The less-defined microphase separation of B9, compared with B8, might be due to the shorter hydrophilic/hydrophobic block length of 10/10 and less hydrophobic nature of *m*BAPPS moieties than BAHF moieties.

The BAPBDS-based multiblock co-SPI membrane B7 exhibited a homogeneous morphology from TEM observation. The formation of microphase separation seemed very difficult for the rigid main-chain-type multiblock co-SPIs as well as the random co-SPIs.

It is noted that not a few papers reported on the presence of microphase-separated structure for sulfonated aromatic PEMs based on only the TEM observation of cluster-like domains. However, it is essential to confirm that the cluster-like domains are really attributed to the hydrophilic domains by means of the EDX analysis of not only stain-metal element content but also S content. Without such an analysis and discussion about the formation of the cluster-like hydrophilic domains from the rigid aromatic polymer chains, the reports would mislead the readers.

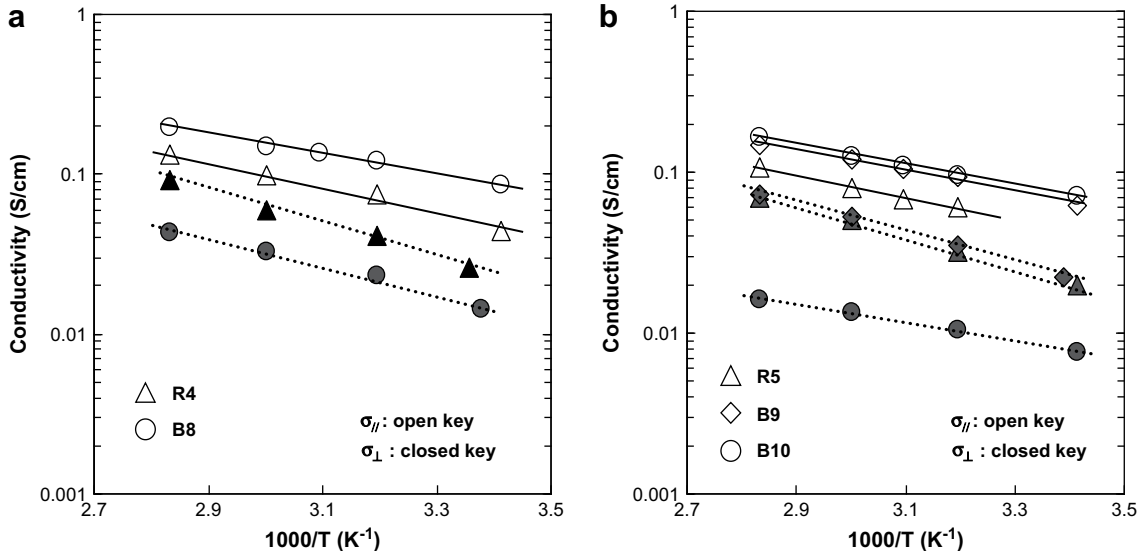

Fig. 8. Temperature dependence of *in-plane* and *through-plane* proton conductivity in water for BSPOB-based multiblock and random co-SPI membranes.

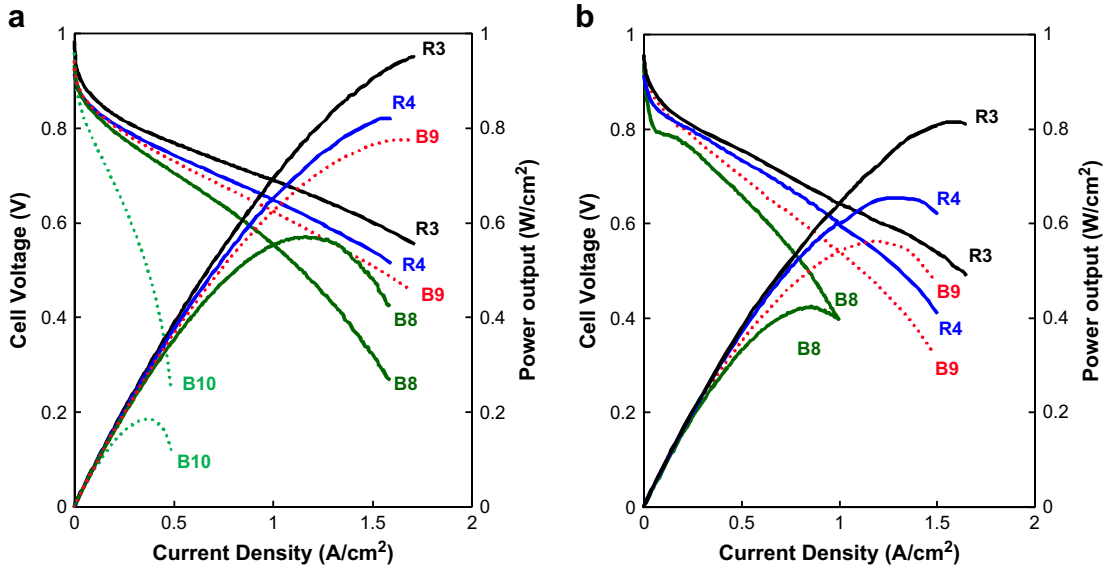

Fig. 9. PEFC performances for BSPOB-based multiblock and random co-SPI membranes B8, B9, B10, R3 and R4 at 90 °C and 0.3 MPa with supply of H_2/air. Humidification temperature: (a) 85 °C and (b) 59 °C.

3.3. Proton conductivity

The *in-plane* proton conductivity ($\sigma_{\parallel}$) at 60 °C as a function of relative humidity is summarized in Table 1 and Fig. 7. The BSPOB-based multiblock co-SPIs (B8–B10) have 1.6–2.4 times larger $\sigma_{\parallel}$ values than the random co-SPIs (R4, R5). Comparison between B9 and B10 with hydrophilic/hydrophobic block length of 10/10 and 20/20, respectively, shows the similar $\sigma_{\parallel}$ values, indicating no clear effect of block length (>10) on the *in-plane* conductivity. This is clearly different from the results reported by Kawakami et al. and Watanabe et al. [28–30]. They reported high $\sigma_{\parallel}$ values of 20 and 25 mS cm^{-1} at 80 °C and 50% RH for the block co-SPIs with very large block lengths of 140/60 and 150/150, respectively. The present $\sigma_{\parallel}$ value of 10 mS cm^{-1} at 60 °C and 50% RH for B8 with block lengths of 20/20 is considered to be comparable to their values, taking high IECs of 2.4 and 1.8 meq g^{-1} and a high temperature into account.

The *through-plane* and *in-plane* proton conductivity ($\sigma_{\perp}$ and $\sigma_{\parallel}$, respectively) and the anisotropic proton conductivity ratio ($\sigma_{\perp/\parallel}$) in water at 60 °C are summarized in Table 2. All the SPI membranes showed anisotropic proton conductivity with larger $\sigma_{\parallel}$ than $\sigma_{\perp}$. Fig. 8 shows the temperature dependence of $\sigma_{\parallel}$ and $\sigma_{\perp}$ in water. In the case of BSPOB-based co-SPIs, the activation energies of $\sigma_{\perp}$ were 16–18 kJ mol^{-1} and slightly larger for those of $\sigma_{\parallel}$ (12 kJ mol^{-1}). The multiblock co-SPIs (B8 and B9-10) exhibited larger $\sigma_{\parallel}$ values and smaller $\sigma_{\perp}$ values and as a result much smaller $\sigma_{\perp/\parallel}$ values than the corresponding random co-SPIs. For example, compared with R4, the $\sigma_{\parallel}$ value of B8 increased by 50%, but its $\sigma_{\perp}$ value decreased by 50% and its $\sigma_{\perp/\parallel}$ value decreased down to a third of that of R4. As mentioned above, R4 had the homogeneous morphology, whereas B8 had the microphase-separated structure with layer-like domains oriented in the plane direction. The difference in the morphology provides a clear explanation on the more significant anisotropic proton conductivity for B8, as mentioned above. Compared with B8 and B10, B9 exhibited a larger $\sigma_{\perp/\parallel}$ value of 0.44 due to the less-defined microphase separation.

In the case of BAPBDS-based co-SPIs, although not being clearly compared because of the different hydrophobic diamine moieties, the $\sigma_{\parallel}$ values were 1.4–1.7 times larger for the multiblock co-SPIs than for the random ones with the similar IECs, whereas the $\sigma_{\perp}$ values were comparable to or slightly larger for the former, and as a result the $\sigma_{\perp/\parallel}$ values were slightly smaller for the former.

The BSPOB-based and BAPBDS-based random co-SPIs showed the homogeneous morphology, but showed the anisotropic proton conductivity due to the polymer chain alignment in the plane direction of membrane. The BSPOB-based co-SPIs showed the slightly smaller $\sigma_{\perp/\parallel}$ values (about 0.65) than the BAPBDS-based ones (0.75) irrespective of the much larger $\Delta_{t/l}$ values of the former.

3.4. Fuel cell performance

Fig. 9 shows the PEFC performances of B8, B9, B10, R3 and R4 at a cell temperature of 90 °C. Table 3 lists the *through-plane* conductivity ($\sigma_{\perp}$), cell voltage at current density of 1.0 A cm^{-2} (V_1)

Table 3
Through-plane proton conductivity ($\sigma_{\perp}$) evaluated from cell resistance, cell voltage at current density of 1.0 A cm^{-2} (V_1) and maximum output (W_{max}) of PEFCs operated at 90 °C, 0.3 MPa and different humidifier temperatures.

PEM code	d (μm)	Humidifier temperature								
		85 °C			72 °C			59 °C		
		$\sigma_{\perp}$ (mS cm^{-1})	V_1 (V)	W_{max} (W cm^{-2})	$\sigma_{\perp}$ (mS cm^{-1})	V_1 (V)	W_{max} (W cm^{-2})	$\sigma_{\perp}$ (mS cm^{-1})	V_1 (V)	W_{max} (W cm^{-2})
B8	42	28	0.55	0.57	24	0.51	0.51	19	0.40	0.42
B9	42	41	0.63	0.79	32	0.61	0.69	22	0.54	0.56
B10	52	8	0.25[a]	0.17						
R3	42	71	0.69	>0.95	63	0.67	0.89	57	0.65	0.82
R4	38	50	0.65	0.82	44	0.63	0.73	41	0.61	0.65

[a] Cell voltage at 0.5 A cm^{-2}.

and maximum output (W_{max}) under the different humidification conditions. The $\sigma_{\perp}$ values were evaluated by complex impedance analysis under PEFC operation by assuming that the cell resistances were mainly attributed to the membrane resistances. Open circuit voltage (OCV) was in the range of 0.97–1.00 V for every SPI membrane except for B10 (0.94 V). The other PEFC performances including the cell voltage and power output at a given current density and W_{max} significantly depended on the SPI membranes. The $\sigma_{\parallel}$ values of multiblock co-SPI membranes B8, B9 and B10 in the humidity range above 50% RH were comparable to or slightly smaller than those of the random one R3 and much larger than those of R4, as listed in Table 1. However, the actually-observed PEFC performances for these SPI membranes were quite different from those expected from the $\sigma_{\parallel}$ values, that is, the PEFC performances were in the order, R3 > R4 > B9 > B8 ≫ B10. This was the same as the order of $\sigma_{\perp}$ values as listed in Table 2.

At a high humidifier temperature of 85 °C (84% RH), R3 showed the highest PEFC performance because of the highest IEC and *through-plane* conductivity. R4 showed the second-highest performance, which was much higher than that of B8. This clearly indicates the much lower PEFC performance of the multiblock co-SPI (B8) compared with the corresponding random one (R4). B9 showed the higher PEFC performance than B8 in spite of the slightly lower IEC. B10 showed the very poor PEFC performance with a very small W_{max} of 0.17 W cm^{-2} at 0.29 A cm^{-2} because of large IR drop.

With decreasing the humidifier temperature from 85 °C to 59 °C (30% RH), the PEFC performance decreased more greatly for the multiblock co-SPIs than for the random ones. The PEFC with B10 could not work at the humidifier temperatures of 72 °C and 59 °C, whereas R3 maintained its PEFC performance at a fairly high level even under a low humidification of 30% RH. Under the low humidification conditions, the membrane still keeps a higher water sorption content than the corresponding equilibrium state with water vapor in the supplied gases, because the water formed at the cathode back-diffuses into the membrane. Judging from the membrane morphology, the *through-plane* water permeation is considered to be lower for the multiblock co-SPIs than for the random ones. The back diffusion of water from the cathode seems less effective for the multiblock co-SPIs, resulting in a lower sorbed-water content in membrane under PEFC operation. Therefore, the much lower PEFC performances for the multiblock co-SPIs are considered due to both the lower *through-plane* proton conductivity and the more dried state of membrane.

The lower PEFC performances of B8, B9 and B10 compared with R3 and R4 were clearly attributed to the lower *through-plane* conductivity under PEFC operation, as listed in Table 3. In the case of the humidification temperature of 85 °C, the $\sigma_{\perp}$ values evaluated reflect the *through-plane* conductivities at about 84% RH, because of the back diffusion of water is less important. At the lower humidification temperatures, the effect of back diffusion of water becomes more important. With decreasing the humidification temperature from 85 °C down to 59 °C, the $\sigma_{\perp}$ values decreased more largely for the multiblock co-SPIs than for the random co-SPIs. This is partly due to the lower water sorption content in membrane as a result of the lower back diffusion of water.

4. Conclusions

Based on the cross-sectional membrane morphology, anisotropic membrane swelling and anisotropic proton conductivity, the co-SPIs studied in this paper are characterized as follows. The BSPOB-based multiblock co-SPIs (B8–B10) exhibited the microphase-separated morphology with hydrophilic and hydrophobic layer-like domains oriented in the plane direction. The layer-like domain structure caused an increase in water uptake, which was followed by an increase in Δt_c and a decrease in Δl_c, whereas it caused an increase in $\sigma_{\parallel}$ and a decrease in $\sigma_{\perp}$. As a result, they showed large $\Delta_{t/l}$ values of about 25 and very small $\sigma_{\perp/\parallel}$ values of 0.10–0.44. These multiblock co-SPIs showed lower PEFC performances than the random co-SPIs because of the lower *through-plane* conductivity.

The BAPBDS-based multiblock co-SPIs (transparent membranes, B5–B7) did not show the microphase-separated morphology from TEM observation. They showed fairly low $\sigma_{\perp/\parallel}$ values of about 0.55, suggest the presence of some kind of aggregation of hydrophilic blocks.

The BSPOB-based and BAPBDS-based random co-SPIs showed the homogeneous morphology, but showed the anisotropic membrane swelling and anisotropic proton conductivity due to the polymer chain alignment in the plane direction of membrane. The former showed the larger $\Delta_{t/l}$ values (6–11) and the slightly smaller $\sigma_{\perp/\parallel}$ values (about 0.65) than the latter (<3 and 0.75, respectively) because the rigid imide backbone from NTDA and BSPOB seemed to cause the better alignment of polymer chain in the plane direction than the less rigid imide backbone from NTDA and BAPBDS.

In summary, multiblock copolymerization is a plausible method to form hydrophilic–hydrophobic microphase-separated morphology for rigid aromatic PEMs. However, the microstructures such as the size, shape and orientation of domains should be controlled preferably to PEMs for PEFC applications. This study demonstrated that such factors must be taken into consideration in the novel block microstructures designs.

Acknowledgements

This work was financially supported by the New Energy and Industrial Technology Development Organization (NEDO) and by a Grand-in-aid for Development Science Research (No. 19550209) from the Ministry of Education, Science, and Culture of Japan. The authors would like to thank Drs. M. Morishima and A. Onuma (Hitachi Ltd., Hitachi Research Laboratory) for performing the STEM experiments.

References

[1] Savagogo O. J New Mater Electrochem Syst 1998;1:47–66.
[2] Mauritz K, Moore R. Chem Rev 2004;104:4535–85.
[3] Hickner M, Ghassemi H, Kim Y, Einsla B, McGrath JE. Chem Rev 2004;104:4587–612.
[4] Rikukawa M, Sanui K. Prog Polym Sci 2000;25:1463–502.
[5] Kerres J. J Membr Sci 2001;185:3–27.
[6] Roziere J, Jones D. Annu Rev Mater Res 2003;33:503–55.
[7] Yin Y, Yamada O, Tanaka K, Okamoto K. Polym J 2006;38:197–219.
[8] Cornet N, Diat O, Gebel G, Jousse F, Marsacq D, Mercier R, et al. J New Mater Electrochem Syst 2000;3:33–42.
[9] Yamada O, Yin Y, Tanaka K, Kita H, Okamoto K. Electrochim Acta 2005;50:2655–9.
[10] Ma S, Siroma Z, Tanaka H. J Electrochem Soc 2006;153:2274–81.
[11] Elabd YA, Napadensky E, Walker CW, Winey KI. Macromolecules 2006;39:399–407.
[12] Tsang E, Zhang Z, Shi Z, Soboleva T, Holdcroft S. J Am Chem Soc 2007;129:15106–7.
[13] Hsu WY, Gierke TD. J Membr Sci 1983;13:307–26.
[14] Storey RF, Baugh III DW. Polymer 2000;41:3205–11.
[15] Yang JE, Lee JS. Electrochim Acta 2004;50:617–20.
[16] Kim B, Kim J, Jung B. J Membr Sci 2005;250:175–82.
[17] Shi Z, Holdcroft S. Macromolecules 2005;38:4193–201.
[18] Xu K, Li K, Khanchaitit P, Wang Q. Chem Mater 2007;19:5937–45.
[19] Haack JM, Taeger A, Vogel C, Schlenstedt K, Lenk W, Lehmann D. Sep Purif Technol 2005;41:207–20.
[20] Ghassemi H, Ndip G, McGrath JE. Polymer 2004;45:5855–62.
[21] Ghassemi H, McGrath J, Zawodzinski Jr T. Polymer 2006;47:4132–9.
[22] Roy A, Hickner MA, Yu X, Li Y, Glass TE, McGrath JE. J Polym Sci Part B Polym Phys 2006;44:2226–39.
[23] Wang H, Badami AS, Roy A, McGrath JE. J Polym Sci Part A Polym Chem 2007;45:284–94.

[24] Lee HS, Badami AS, Roy A, McGrath JE. J Polym Sci Part A Polym Chem 2007;45:4879–90.
[25] Lee HS, Roy A, Badami AS, McGrath JE. Macromol Res 2007;15:160–6.
[26] Schönberger F, Kerres J. J Polym Sci Part A Polym Chem 2007;45:5237–55.
[27] Nakabayashi K, Matsumoto K, Ueda M. J Polym Sci Part A Polym Chem 2008;46:3947–57.
[28] Nakano T, Nagaoka S, Kawakami H. Polym Adv Technol 2005;16:753–7.
[29] Nakano T, Nagaoka S, Kawakami H. Kobunshi Ronbunshu 2006;63:200–4.
[30] Yasuda T, Li Y, Miyatake K, Hirai M, Nanasawa M, Watanabe M. J Polym Sci Part A Polym Chem 2006;44:3995–4005.
[31] Watari T, Fang J, Guo X, Tanaka K, Kita H, Okamoto K, et al. J Membr Sci 2004;230:111–20.
[32] Suto Y, Yin Y, Kita H, Okamoto K. J Photopolym Sci Technol 2006;19:273–4.
[33] Suto Y, Yin Y, Hu Z, Chen S, Kita H, Okamoto K, et al. J Polym Sci Part A Polym Chem 2009;44:1463–77.
[34] Guo X, Fang J, Harada S, Watari T, Tanaka K, Kita H, et al. Macromolecules 2002;35:6707–13.
[35] Chen S, Yin Y, Tanaka K, Kita H, Okamoto K. Polymer 2006;47:2660–9.
[36] Hu Z, Yin Y, Kita H, Okamoto K, Suto Y, Wang H, et al. Polymer 2007;48:1962–71.